International Journal of Environmental Science and Technology (2023) 20:1007–1018
https://doi.org/10.1007/s13762-022-04026-w

ORIGINAL PAPER

Surface-functionalized spongy zinc ferrite as a robust visible-light driven nanocatalyst for wastewater remediation: characterization, kinetic, and mechanistic insight

L. Fei[1] · **F. Ali**[2] · **A. Said**[2] · **N. Tariq**[2] · **F. Raziq**[3] · **N. Ali**[1] · **U. Arif**[2] · **M. S. Akhter**[4] · **A. Rahdar**[5] · **M. Bilal**[6]

Received: 18 December 2021 / Revised: 29 January 2022 / Accepted: 8 February 2022 / Published online: 6 March 2022

Abstract

Three different types of zinc ferrite nanoparticles ($ZnFe_2O_4$ NPs) were successfully synthesized through the co-precipitation route. The synthesized $ZnFe_2O_4$ NPs were structurally characterized by Fourier transform infrared (FT-IR), Scanning electron microscopy (SEM), X-ray diffraction (XRD), and Brunauer Emmet Teller spectroscopic analyses. FT-IR analysis confirmed that the (3-APTES) is well grafted on the $ZnFe_2O_4$ NPs surface. XRD analysis shows the crystalline structure of calcined and modified $ZnFe_2O_4$ NPs, while the amorphous nature of bare $ZnFe_2O_4$ NPs was observed. SEM micrographs displayed a flat surface morphology with almost monodispersed grain size and irregular shape structure for all $ZnFe_2O_4$ NPs. The grain size of the synthesized $ZnFe_2O_4$ NPs was found to be 106.5, 23.3, and 13.9 nm for bare, calcined, and modified $ZnFe_2O_4$ NPs, respectively. Optical bandgap energy (LUMO–HOMO gap) was experimentally calculated in acidic and basic mediums (2.47 and 2.70 eV) using a taulc plot. The photocatalytic performance of the synthesized $ZnFe_2O_4$ NPs was investigated under visible irradiation in an aqueous medium against bromophenol blue dye. The influence of various parameters like irradiation time, photocatalyst dose, dye dose, pH effect, and H_2O_2 on the degradation efficiency was investigated. Results showed that all the three types of $ZnFe_2O_4$ NPs exhibited excellent photocatalytic properties, where the highest degradation (95.4%) was displayed by modified $ZNFe_2O_4$ NPs, followed by calcined (90.2%) and bare $ZnFe_2O_4$ 84.6%). The synthesized $ZnFe_2O_4$ NPs were reused and recycled, retaining the excellent photocatalytic property for four consecutive cycles. Kinetic models demonstrate that the degradation rate was pseudo 1st order of kinetics. The turnover number reached up to 21.3×10^6, 22.5×10^6, and 23.8×10^6 for bare, annealed, and functionalized $ZNFe_2O_4$ nanoparticles, respectively. In short, the developed spongy zinc ferrite nanoparticles indicate a high potential of photo-driven catalytic remediation of tested bromophenol blue drained into the water systems.

Keywords Spongy zinc ferrite · Surface morphology · Grafting · Optical bandgap · Nanospheres · Photocatalysis · Remediation

Introduction

Dyes are among the most prominent organic pollutants polluting the aqueous environment (Fuku et al. March 2017; Rauf and Ashraf 2009). Various industries discharge large amounts of dyes into the water worldwide. Removing these dyes from water and wastewater is an environmental priority because mostly, these dyes are resistant to bacteriological decomposition (Nezamzadeh-Ejhieh and Banan 2012). Water pollution is a serious problem as it affects human health. More than 4-million people are annually dying from infections caused by microorganisms, and most of them are caused by water pollution (Nezamzadeh-Ejhieh and Moazzeni 2013; Buthiyappan et al. 2016). So, eliminating biological and chemical pollutants from contaminated water is a challenging task. To remove dyes from textile wastewater, it is essential to search for an effective wastewater treatment process (Magdalane et al. 2017). Various chemical and physical methods, such as adsorption, separation of pollutants, electrocoagulation, chemical precipitation, etc., (Bouanimba et al. 2011; Anchieta et al. 2014) are currently used for wastewater treatment. However, the fundamental limitations

---

Editorial responsibility: Shahid Hussain.

✉ L. Fei
liufei@hyit.edu.cn

Extended author information available on the last page of the article

of these methods are that they are not effective because only contaminants relocate from one phase to another; therefore, different, and new kinds of contamination are faced, and additional treatment is deemed necessary (Rishikeshi et al. 2013). Advanced oxidation process (AOPs) (Buthiyappan et al. 2016), is an alternative conventional method, which works based on the generation of large reactive groups like OH, that non-selectively and quickly oxidizes a broad range of organic contaminants (Khan et al. 2015; Nezamzadeh-Ejhieh and Banan 2011).

The photocatalytic application of $ZnFe_2O_4$ NPs is explored under visible-light irradiation against the decolorization of bromophenol blue. Due to its polar nature, it is a highly water-soluble dye and can be originated in the effluents of textiles, pharmaceuticals, and chemical industries (Dlamini et al. 2011; Haider et al. 2011). To find a close association among shape and various properties, $ZnFe_2O_4$ NPs with diverse morphology, such as multi-porous bricks, nanorods, nanoplates, nanocubes, nanoparticles, etc., have been synthesized by multiple researchers (Srinivasan et al. 2016). Cao et al. (2009) prepared $ZnFe_2O_4$ nanoparticles for the degradation of phenol by Microwave-hydrothermal ionic liquid (MHIL) method that exhibit up to 73% photocatalytic activity within 30 min. Li et al. (2010) developed $ZnFe_2O_4$ nanospheres via the solvothermal route. Under Xe-lamp, the photocatalytic removal efficiency of Rhodamine B (RhB) was 84% after 4 h of irradiation. Xie, Taiping, et al. (Xie et al. 2013) synthesized $ZnFe_2O_4/SrFe_{12}O_{19}$ through a one-step chemical co-precipitation route and studied the photocatalytic activity of composite against the removal of methylene blue under UV-irradiation. The removal rate of composites was greater than 70% after being reused for 4-times. Li, Xinyong, et al. (He et al. 2017) prepared $ZnFe_2O_4$ nanospheres via solvothermal route, and under xenon-lamp irradiation, the photocatalytic degradation efficiency of RhB reached 85% after 3 h.

Neshin et al. (2021) reported Ni-doped $BiFeO_3$ NPs for degradation of BPB in aqueous media. Their photocatalyst efficiency was recorded as 85.76% (Mohsen et al. 2021). Similarly, Humayun Khan et al. (2016) reported Chitosan conjugated magnetic (Ni-CCMN) NPs for the degradation of BPB. They reported that the photocatalyst could degrade BPB up to 83% (Khan et al. 2016). Ameen et al. (2014) synthesized CeO_2/TiO_2 nanocomposite as a visible-light photocatalyst for the degradation of BPB. They observed that the prepared photocatalyst can degrade BPB up to 72% (Ameen et al. 2014). Shah et al. (2019) reported TiO_2/GNP nanoplatelets for the degradation of BPB. The observed efficiency was 86% (Shah et al. 2019). Emmanuel et al. (2021) reported Clinoptilolite/Activated Carbon for the degradation of BPB. The observed efficiency was 80.0% for the degradation/ removal of BPB (Emmanuel and Sudesh 2021). In comparison, we synthesized spongy $ZnFe_2O_4$ NPs by co-precipitation method, which is simple and cost-effective. We recorded that the spongy $ZnFe_2O_4$ photocatalyst has a degradation efficiency of greater than 95%.

Different groups synthesized and investigated zinc ferrite $ZnFe_2O_4$ NPs as photocatalysts for the degradation of different dyes. But more salts (organic) contents are used in reactions to having microstructure morphology at expensive costs. Secondly, lots of waste materials are also produced as a byproduct (Fan et al. 2009). Therefore, environment-friendly, easy, and fast methods like sol–gel, hydrothermal, ball mill, sonication, co-precipitation, etc., are mostly preferred for the synthesis of $ZnFe_2O_4$ NPs nanostructures. Herein, we prefer the method of co-precipitation for the synthesis of spongy zinc ferrite $ZnFe_2O_4$ nanocatalyst/photocatalyst. Spongy $ZnFe_2O_4$ photocatalyst is gaining more attention due to their excellent applications as gas sensor, mechanical properties, electric nature, and most importantly, their Photocatalysis character. Spongy $ZnFe_2O_4$ photocatalyst shows good optical absorption due to its narrow bandgap of about 1.9 eV (Cao et al. 2009). Due to their magnetic properties, these spongy photocatalysts can be reused again and again as effective photocatalysts to eliminate industrial organic pollutants (Fu and Wang 2011).

The spongy nanostructures were passed through calcination at high temperatures, i.e., 1000 °C, and hydroxylation treated with 1 M HCl. It has been noticed that the surface properties of the photocatalyst become more efficient after treating with 3-(triethoxysilyl) propylamine. Different characterization confirmed the enhanced properties and morphology of the ZnFe2O4 nanostructures zinc ferrite ZnFe2O4 nanostructures. In this research study, the degradation of Bromophenol blue (BPB) dye was investigated using these synthesized spongy zinc ferrite photocatalyst. Bromophenol Blue (BPB) dye is used to examine the efficiency and photo-degradation of the synthesized photocatalyst. Marvelously, BPB shows 95.4% degradation at pH-12 in 2 h. Diverse parameters have been investigated; kinetics models were applied, demonstrating that the degradation process was pseudo 1^{st} order kinetics. The catalytic performance concerning turnover frequency (TOF) or turnover number (TON are estimated to measure the activities of different catalysts in numerous disciplines of heterogeneous, homogeneous, and nanocatalysis.

Materials and methods

Reagents

Zinc sulfate (≥ 99%), iron sulfate (≥ 97%), triethylene glycol (≥ 99%), sodium hydroxide (≥ 95%), hydrochloric acid (≥ 97%), (3-APTES) (≥ 99%), ascorbic acid (≥ 99.9%), benzoquinone (≥ 98%), 1,4-diazabicyclo[2.2.2]octane

(DABCO) (≥ 98%), and bromophenol blue dye were purchased from Sigma Aldrich and used as received without further purification.

Preparation of $ZnFe_2O_4$ NPs

Zinc ferrite NPs were successfully prepared through the co-precipitation route by the reaction of iron sulfate ($FeSO_4$) (1.822 g, 12 mM) and zinc sulfate ($ZnSO_4$) (0.538 g, 3 mM) in 100 ml of deionized water. Then 50 mM TEG solution was mixed for 2 h with vigorous stirring under ambient conditions. 10 M solution of NaOH was added dropwise into mixed salts mixture to maintain the pH up to 8.0. On this pH, a reddish-brown colored precipitate was achieved, centrifuged, and rinsed several times with distilled water followed by drying for 24 h at 80 °C and mechanically ground into powder. The bare $ZnFe_2O_4$ NP was thermally heated at 1000 °C for 6 h in the furnace. It was noted that the triethylene glycol stabilized $ZnFe_2O_4$ NPs at the interface due to the OH group of glycols, which may oxidize and make a complex with d-block elements, which may oxidize making a complex with the transition metal (Rishikeshi et al. 2013; Ruttink et al. 2012). The formation of $[ZnFe_3O(OAc)_2(H_2O)_3)]$ complex following the formation and reduction of $ZnFe_2O_4$ NPs on heating is also explained (Skrabalak et al. 2008).

Surface modification of $ZnFe_2O_4$ NPs

The thermally treated calcined $ZnFe_2O_4$ NPs were surface modified in two steps. In the initial step, the calcined $ZnFe_2O_4$ NPs were immersed in one molar hydrochloric acid solution under vigorous stirring for 30 min, centrifuged, and washed several times with deionized water. Secondly, 1 g hydroxylated $ZnFe_2O_4$ NPs were treated with 0.1 M solution of 3-(APTES) under vigorous stirring at 60 °C for 2 h, filter off, and drying at 80 °C 24 h and obtained the modified $ZnFe_2O_4$ NPs.

Photocatalytic degradation of bromophenol blue

The optimum amount (i.e., 30 mg) of photocatalysts was dispersed in 50 mL of dye solution (20 ppm) in a flask in each reaction. The mixture was stirred in the dark for 30 min to establish adsorption/desorption equilibrium. A 300 W Xenon lamp equipped with a 420 nm UV-cutoff filter was used as the light source. The lamphouse was well-ventilated so that room temperature was maintained. After every certain time, 5 ml of the reaction solution was centrifuged, and the concentration of the dye was measured using Agilent Cary 60 UV–vis spectrophotometer. The pH values of the solutions were 6.1 and did not change during the degradation reactions.

Influence of irradiation time

The effect of irradiation contact time on the photocatalytic degradation of BPB was investigated. A known concentration solution of BPB was illuminated with a 300 W Xenon lamp equipped with a 420 nm UV-cutoff filter for various irradiation times ranging from 30 to 180 min. The illuminated solution was centrifuged at 4000 rpm for 20 min, and percent degradation was examined through Agilent Cary 60 UV–vis spectrophotometer.

Influence of photocatalyst

The influence of catalyst dose was measured against BPB dye using the various amount of catalyst doses ranging from 10, 15, 20, 25, 30, and 35 mg, respectively. For this purpose, the BPB dye solution was stirred in the dark for 30 min to establish an adsorption/desorption equilibrium and then illuminated with a 300 W Xenon lamp equipped with a 420 nm UV-cutoff filter for the optimized duration (i.e., 120 min). The illuminated solution was centrifuged at 4000 rpm for 20 min, and the percent degradation was examined through Agilent Cary 60 UV–vis spectrophotometer.

Influence of dye

The influence of BPB concentration on the photocatalytic decolorization of BPB was measured using different dye concentrations ranging from 2, 10, 15, 20, 25, 30, 35, and 40 ppm. Initially, 100 ppm stock solution of BPB was prepared. The λmax for BPB measured was at 590 nm. For this purpose, the BPB dye solution was treated in the dark for 30 min and then illuminated with a 300 W Xenon lamp equipped with a 420 nm UV-cutoff filter for the optimized duration. The illuminated solution was centrifuged at 4000 rpm for 20 min, and the percent degradation was examined through Agilent Cary 60 UV–vis spectrophotometer.

Influence of pH

To check the influence of pH on the photocatalytic decolorization of BPB dye. For this purpose, prepared BPB solutions with various pH (i.e., 1–14), the BPB dye solutions with various pH were treated for 30 min in the dark and then illuminated with 300 W Xenon lamp equipped with a 420 nm UV-cutoff filter for the optimized duration (with optimized photocatalyst and dye dose). The illuminated mixture was centrifuged at 4000 rpm for 20 min, and the degradation was examined through Agilent Cary 60 UV–vis spectrophotometer.

Influence of H_2O_2

The influence of solvent on the photocatalytic degradation of BPB was measured using various amount of H_2O_2 (i.e., 1–6 ml). For this purpose, the BPB dye solutions with H_2O_2 were treated for minutes in the dark and then illuminated with visible light under optimum conditions. The illuminated mixture was centrifuged at 4000 rpm for 20 min, and degradation was examined through Agilent Cary 60 UV–vis spectrophotometer.

Turnover frequency (TOF) and turnover number (TON)

In catalysis, it's normal to estimate the catalytic performance concerning turnover frequency (TOF) or turnover number (TON). The TOF and TON are estimated to measure the activities of different catalysts in numerous disciplines of heterogeneous, homogeneous, and nanocatalysis. The coupling product yields 85.4 percent, 90.2 percent, and 95.4 percent for the bare, annealed, and functionalized $ZnFe_2O_4$ nanoparticles, respectively, with turnover frequencies (TOF) of 1186.11, 1252.77, and 1325. The turnover numbers for bare, annealed, and functionalized $ZnFe_2O_4$ nanoparticles reached 21.3×10^6, 22.5×10^6, and 23.8×10^6, respectively.

Results and discussion

Fourier transform infrared (FT-IR) analysis

FT-IR analysis of the prepared $ZnFe_2O_4$ NPs is shown in Fig. 1. In FT-IR spectra of bare $ZnFe_2O_4$ NPs, three small characteristic peaks occur at 3175, 3015, and 1638 cm^{-1}, attributed to the hydroxyl bond (OH) of triethylene glycol (TEG) (Akpan and Hameed 2009). The bond at 1505 cm^{-1} corresponds to the stretching vibration of C–O of TEG, which confirmed the existence of TEG group. These bonds further explain the contract of oxygen of C–O with the iron or zinc on the $ZnFe_2O_4$ surface (Ali et al. 2020a), while the stretching vibration band of Zn–O and Fe–O is observed at 605 and 685 cm^{-1}, respectively (Hankare et al. 2011). The disappearance of bands at 3175 and 3015 cm^{-1} in FT-IR spectra of calcined $ZnFe_2O_4$ NPs is a clear indication that there is no more hydroxyl group, which shows that there are no more water molecules (Ali et al. 2020a). A small band at 1412 cm^{-1} corresponds to the bending vibration of the –COO^{-} group (Ali et al. 2020b), and the band at 861 cm^{-1} corresponds to the C–H bending vibration (Yang et al. 2014). The bands at 644 and 527 cm^{-1} are attributed to the bending vibration of ZnO (Sakthivel et al. 2003), while the band 446 cm^{-1} corresponds to the Fe–O bond (Tourinho et al. 2007). The FT-IR spectra of modified $ZnFe_2O_4$ NPs are entirely different from the bare and calcined $ZnFe_2O_4$ NPs. The vibration peak of O–H of water molecule was observed at 3342 (Ali et al. 2020c), and 3281 cm^{-1}, and the bands at 2937 and 2848 cm^{-1} correspond to the vibration of $CH_2CH_2CH_2NH_2$ (Ali et al. 2020c), which confirmed that the 3-(APTES) is well grafted on the $ZnFe_2O_4$ NPs surface (Ali et al. 2020c). The binding and stretching vibration of N–H and C–H of $-CO_2^-$ group shows the bands at 1582 and 1462 cm^{-1}, respectively (Shams-Ghahfarokhi and Nezamzadeh-Ejhieh 2015). The stretching vibration peaks of N–O of NO_3^- group occurred at 987 and 909 cm^{-1} (Ali et al. 2020d). The binding vibration bands C-H occurred at 748 cm^{-1} (Bouanimba et al. 2011), while the bands at 679 and 532 cm^{-1} correspond to the vibration of Zn–O (Posa et al. 2016) & Fe–O (Li et al. 2011), respectively.

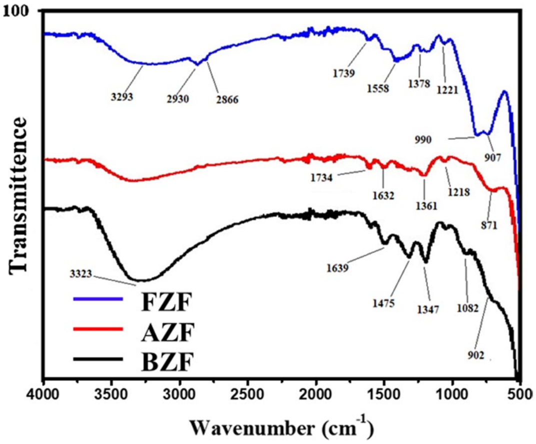

Fig. 1 FTIR analysis of functionalized, annealed, and bare $ZnFe_2O_4$

X-ray diffraction (XRD) analysis

The structural morphology of the synthesized spongy $ZnFe_2O_4$ NPs was investigated through the XRD pattern shown in Fig. 2. The peaks of XRD have been examined and inspected by using the software X'Pert High score (JCPDs No: 73-1963). The XRD diffraction pattern illustrated that all the recorded peaks are reasonably matched with the cubic structure of Zinc Ferrite nanoparticles (Ullah et al. 2018). By using the Scherer formula, average crystallite size has been calculated (Ali et al. 2020c).

$$S = \frac{K\lambda}{B\mathrm{Cos}\theta} \tag{1}$$

Here, S is the grain size, K is constant, having the value of 0.94, λ is wavelength having the value of 1.5406 Å, B is the FWHM, where θ is the diffraction peak position. Bare $ZnFe_2O_4$ NPs do not show any intense diffraction peak at (2θ) as illustrated in Fig. 2, demonstrating the amorphous character. On the other hand, annealed and functionalized

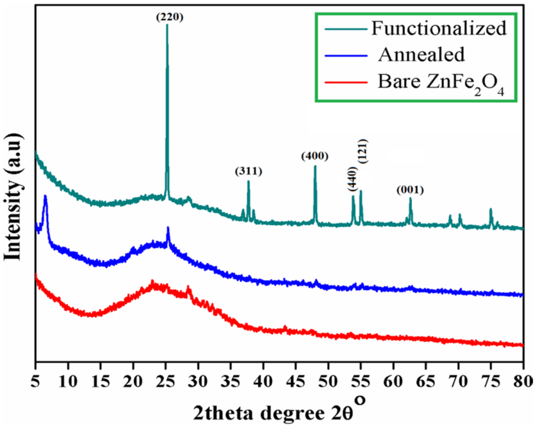

Fig. 2 XRD graphs of functionalized, annealed, and bare $ZnFe_2O_4$ nanoparticles

NPs show intense diffraction peaks at 25.4, 37.8, 48.2, 53.9, and 54.6 2theta degree, corresponding to the reflective plane (220), (311), (400), (440), and (121), respectively, show the crystallinity in modified NPs (Ali et al. 2020a). The calculated grain size for bare $ZnFe_2O_4$, annealed $ZnFe_2O_4$, and modified $ZnFe_2O_4$ NPs are 106.5, 23.3, and 13.9 nm, respectively (Sehar et al. 2019). The XRD diffraction pattern for $ZnFe_2O_4$ NPs provides various information about peak position, d-spacing values, maximum height values, and full width and half maximum values. The average grain size for all three types of NPs was calculated by using the Scherrer calculator.

Scanning electron microscopy (SEM) analysis

SEM spectroscopy was used to get the definitive evidence of the shape and structural morphology of the prepared zinc ferrite $ZnFe_2O_4$ NPs as illustrated in Fig. 3a–l. SEM micrograph of $ZnFe_2O_4$ NPs (bare, calcined, and functionalized), respectively, exhibit the formation of distinct morphology of the prepared nanoparticles. The SEM micrographs of bare or blank $ZnFe_2O_4$ NPs display the homogeneous dispersion of grain with an aggregate of big spheres of about 1 µm as shown in Fig. 3a–d. SEM results showed a spherical shape in a cluster, and these SEM micrographs of bare ZnFe2O4 NPs showed irregular shape and size. The surface morphology of calcined $ZnFe_2O_4$ NPs appears more homogeneous, and the average surface roughness has been estimated to be slighter lesser than $ZnFe_2O_4$ NPs as shown in Fig. 3e–h. The high thermal treatment of the bare $ZnFe_2O_4$ NPs leads to the removal of water molecules, and the organic species, such as TEG and its oxidizing product, is the reduction of bare $ZnFe_2O_4$ NPs (Jadhav et al. 2011). The high thermal treatment promotes the nucleation and growth of $ZnFe_2O_4$ NPs, leading to the integration of smaller particles to produce a

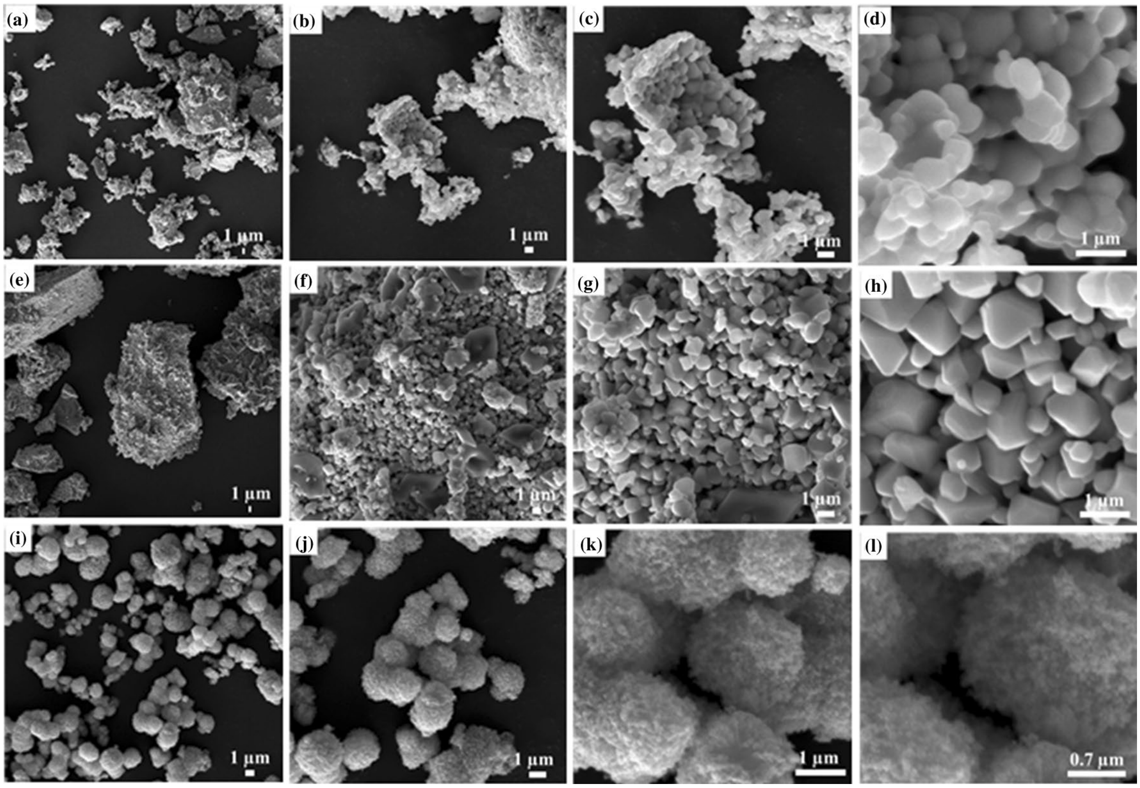

Fig. 3 Scanning electron micrographs (SEM) of **a–d** Bare $ZnFe_2O_4$, **e–g** annealed $ZnFe_2O_4$, and **i–l** functionalized $ZnFe_2O_4$

greater aggregate of structure and agglomerations due to annealing occurred more in calcined NPs of $ZnFe_2O_4$, where the particles in the range of 0.7 µm and big spongy materials were formed (Dehghani et al. 2017). The surface modification procedure contains hydroxylation of calcined-$ZnFe_2O_4$ NPs, which leads to the departure of roughly bound crystallite in calcined bunches of NPs and hydroxylation of the surface of the NPs. The $ZnFe_2O_4$ NPs having OH sorts were treated with 3-(APTES). The SEM micrographs of modified $ZnFe_2O_4$ NPs, as illustrated in Fig. 3i–l shows that the higher aggregation of nanospheres vanishes, the grain's overall dispersion is improved after modification, and spherical particles are more closely packed and interacted in modified NPs of $ZnFe_2O_4$. A reduction in the size of Fe_2O_4 NPs after the oleic acid modification has been previously reported that having similar reasons (Dhiman et al. 2016).

Thermogravimetric analysis

Thermogravimetric analysis (TGA) of blank, annealed and functionalized $ZnFe_2O_4$ NPs shown in Fig. 4. Thermo graph of blank and functionalized $ZnFe_2O_4$ NPs shows two steps thermal degradation pattern, first weight loss (WL1) at 100–150 °C due to the evaporation of water and solvent molecules. The second and final weight loss (WL2) because of decomposition of the main backbone of $ZnFe_2O_4$ take place at about 435 and 452 °C for blank and functionalized $ZnFe_2O_4$ NPs. Thermal stability of annealed $ZnFe_2O_4$ NPs shows one-step weight loss, which occurred at a temperature of 490 °C, because of decomposition of the SO3H group of the membrane as a report.

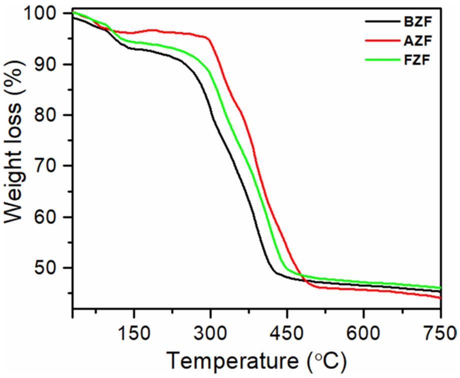

Fig. 4 TGA analysis of the synthesized bare, annealed, and functionalized $ZnFe_2O_4$ NPs

The optical property of $ZnFe_2O_4$ NPs

Diffuse reflectance spectroscopy was used to study the ultraviolet–visible absorption of $ZnFe_2O_4$ NPs Fig. 5. $BaSO_4$ was used as a blank, and absorbance was expressed by treating the reflectance data with the Kubelka–Munk function. According to the UV absorption edges of 506, 530, and 545 nm for blank, annealed, and functionalized $ZnFe_2O_4$ NPs, corresponding to the bandgap of 2.37, 2.28, and 2.22 eV for blank, annealed, and functionalized $ZnFe_2O_4$ NPs, respectively.

Photocatalytic activities $ZnFe_2O_4$ NPs

Effect of illumination time

The amount of $ZnFe_2O_4$ NPs as 10 mg was fixed to investigate the relationship between illumination time and photocatalytic degradation efficiency of BPB, and the results are illustrated in Fig. 6. The results show that with increased illumination time, the degradation efficiency increase. In the heterogeneous catalyst, the OH ions are extremely accepted as primary oxidants (Jayaraman et al. 2012). The $OH^{•}$ radical have strong oxidizing power, which is enough to oxidize the adsorbed dye molecules on the surface of $ZnFe_2O_4$ NPs into the water, CO_2, and other minerals acid (Khan et al. 2016; Jayaraman et al. 2012). Only a small increment of photocatalytic degradation efficiency was observed when the contact time was longer than 120 min. The probable reason is when enhancing the illumination time, a large

Fig. 5 Taulc plots for calculation of bandgap energy of $ZnFe_2O_4$ NPs

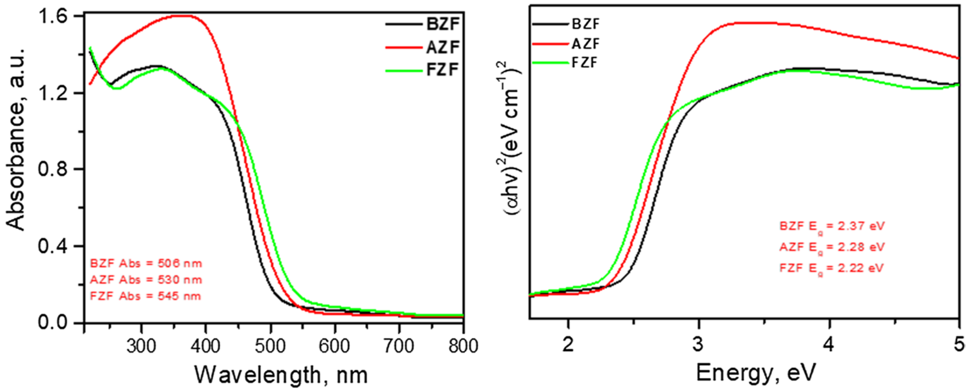

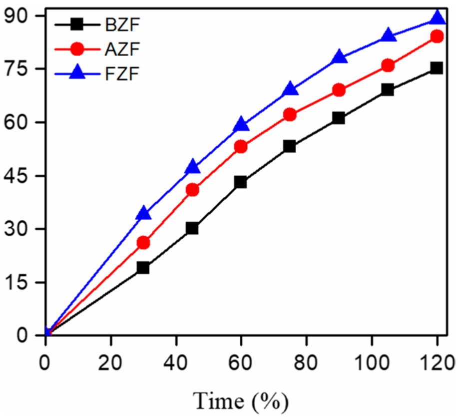

Fig. 6 Effect of irradiation time on the degradation of BPB using bare, annealed, and functionalized $ZnFe_2O_4$ nanoparticles

number of little organic molecules are produced by photogeneration, and small organic molecules are degraded by the surface of $ZnFe_2O_4$, resulting in a decrease in the formation of hydroxyl radicals that attack the dye molecules; therefore, the dose does not lead to greater photo-degradation efficiency of BPB with an increase in irradiation time (Jia et al. 2011).

Influence of photocatalyst dose

The influence of catalyst dose on the photocatalytic decolorization of BPB was examined by using different amounts of photocatalyst ranging from 5 to 35 mg at the concentration of a fixed dye under UV–visible light. The catalyst degradation efficiency load on BPB is shown in Fig. 7, which shows that the efficiency is greatly increased by enhancing the concentration of catalyst from 10 to 35 mg. After this, the decolorization rate remains almost constant, and the highest degradation has occurred at 30 mg of $ZnFe_2O_4$ NPs; similar results were achieved by other workers (Ali et al. 2020c). The number of the active site on the surface of $ZnFe_2O_4$ NPs increase with the increase in the amount of catalyst by increasing the number of $O_2^{-\bullet}$ and $OH^{\bullet}$ radicals (Hankare et al. 2011). At the same period with a large dose of photocatalyst, the turbidity of the mixture increase, and the photo-activated volume of suspension decrease because of a reduction in the penetration of VU-radiation (Yang et al. 2014). Thus, it can be determined that a high catalytic dose may not be valuable both because of accumulation is well as reduced irradiation field due to the radiation scattering (Jia et al. 2011).

Effect of dye concentration

The influence of dye concentration is one of the vital parameters, which affect the photocatalytic rate of BPB dye. On the removal of BPB dye, the influence of dye concentration showed that the highest decolorization occurs at 5 ppm of the dye solution, and then the degradation rate is reduced with increased dye dose, as shown in Fig. 8. The photocatalytic decolorization rate of BPB dye is because increased dye dose causes greater interaction of radiation with dye molecules, and radiation is unable to contact with catalyst surface; as a result, the rate of dye degradation decrease (Xie and Li 2006). High dye molecules produce many inorganic ions, such as nitrate & sulfate ions in a mixture that competes with dye molecules (Ali et al. 2020a). According to Bear-Lambert law (Ali et al. 2020c; Tashtoush 2021), when the amount of solution increase, the path length of incoming photons to solution molecules reduce, causing fewer numbers of photons to approach the photocatalyst surface and cause smaller degradation of dye molecules (Ali et al. 2020c).

Influence of solution pH

The influence of pH plays a key role in controlling the photocatalytic decolorization of dye on the photocatalyst surface. The pH values of the BPB solution were controlled by using

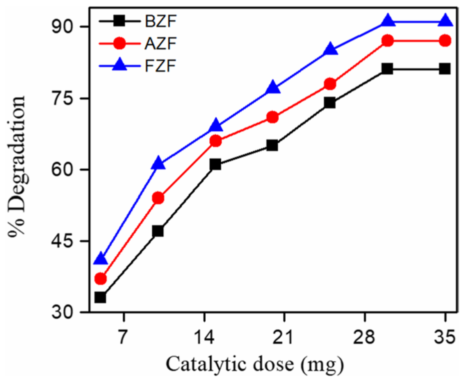

Fig. 7 Effect of catalytic dose on the degradation of BPB

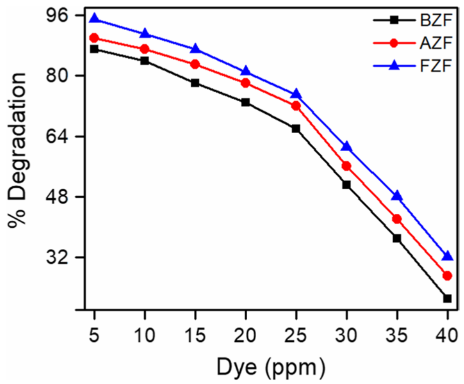

Fig. 8 Effect of dye dose on the degradation of BPB

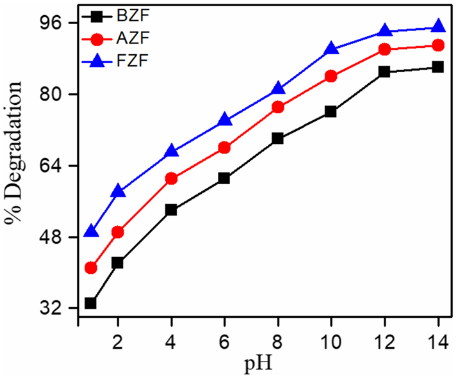

Fig. 9 Effect of solution pH on the degradation of BPB

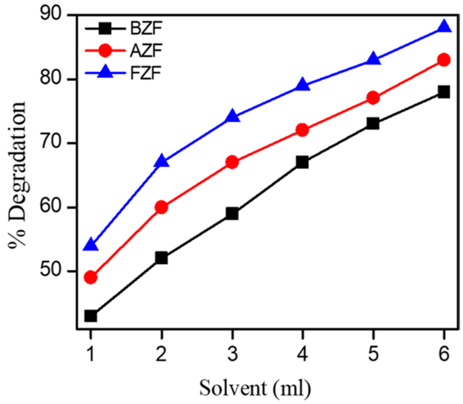

Fig. 10 Effect of H_2O_2 on the degradation of BPB

NaOH and HCl, and the achieved results are illustrated in Fig. 9. It was recorded that the photocatalyst showed the maximum photocatalytic activity at pH 12–14. In this, the Cl^- anion can react with hydroxyl radical leading to inorganic smaller reactivity than $OH^•$, so they do not participate in the degradation of BPB molecules. There is also a drastic competition among the dye molecules and anions concerning $^•OH$ radicals. A higher concentration of OH ions may lead to the deactivation of radicals (Ali et al. 2020c). Initially, the water and $H_2O_2^•$ were formed due to the reaction of hydroxyl-hydroxyl radicals. The reactivity of these radicals with dye molecules is very rare as compared to OH radicals. Secondly, due to the availability of a high amount of OH radicals; the radical–radical reaction occurs at a higher pH value (Ali et al. 2020a).

Influence of H_2O_2

The influence of H_2O_2 on the degradation of BPB is summarized in Fig. 10. It exhibits that the photocatalytic degradation of BPB on $ZnFe_2O_4$ NPs increases with increasing H_2O_2 concentration. With a rise in the H_2O_2 concentration, the degradation rate increases due to the presence of a greater number of hydroxyl radicals, which increase the degradation process by attacking the aromatic rings (Akpan and Hameed 2009). Due to the formation of $HO_2^•$, the degradation rate is decreased when the hydroxyl radicals are maximum, it reacts with H_2O_2 then $HO_2^•$ is formed. $HO_2^•$ is less effective a hydroxyl and when $HO_2^•$ is increasing, it has negligible contribution in dye destruction, which might result in lower degradation (Wu et al. 2016).

Mechanism of photocatalysis and recycling

To understand the degradation mechanism, the functions of superoxide ($O_2^{•-}$), singlet oxygen ($^1O_2$), hole (h^+), and hydroxyl radical ($^•OH$) in the degradation of BPB were investigated. Notably, benzoquinone is an $O_2^{•-}$ quencher, DABCO is a $^1O_2$ quencher, ascorbic acid and isopropanol are the quenchers of both hole and $^•OH$. Here, the influence of these quenchers on the photo-degradation of BPB was investigated. As shown in Fig. 11, all benzoquinone, ascorbic acid, and isopropanol caused the degradation rate of BPB to decrease drastically, while DABCO did not affect the rate. Hence, all $O_2^{•-}$ and hole (h^+) and hydroxyl radical ($^•OH$) were involved in the photo-induced degradation of BPB, and meanwhile $O_2^{•-}$ should not be involved in the degradation reaction. By analysis of the degradation rates, it could be found that the degradation rates with benzoquinone, ascorbic acid, and isopropanol, respectively, were ca. 17%, 34%, and 45% of that without additive. Therefore, the degradation of the dyes under visible light irradiation should follow the sensitization mechanism, and $O_2^{•-}$, hole (h^+) and hydroxyl radical ($^•OH$) played a significant role in the degradation. The recycling experiments showed that ZnFe2O4 NPs still held excellent activity after five successive cycles. The removal efficiency decreased slightly to ca. 83.4% in the fifth run Fig. 12. The slight decrease of the activity may presumably be attributed to the loss of the catalyst.

Kinetic study of photocatalytic degradation of BPB

Kinetics studies are very important to know the mechanism of dye molecules. The reaction kinetics of photocatalytic degradation of BPB using bare, calcined, and modified $ZnFe_2O_4$ NPs are shown in Fig. 13. The reaction kinetics were determined from various irradiation times. Then plot the 1 + log of optical density against radiation time, giving a straight line with R^2 value 0.931, 0.960, and 0.981 (bare, annealed, and modified) $ZnFe_2O_4$ NPs, respectively, that implies the degradation reaction pseudo-first-order of kinetics, and the constant rate value is 2.303 × slope (Valizadeh et al. 2016).

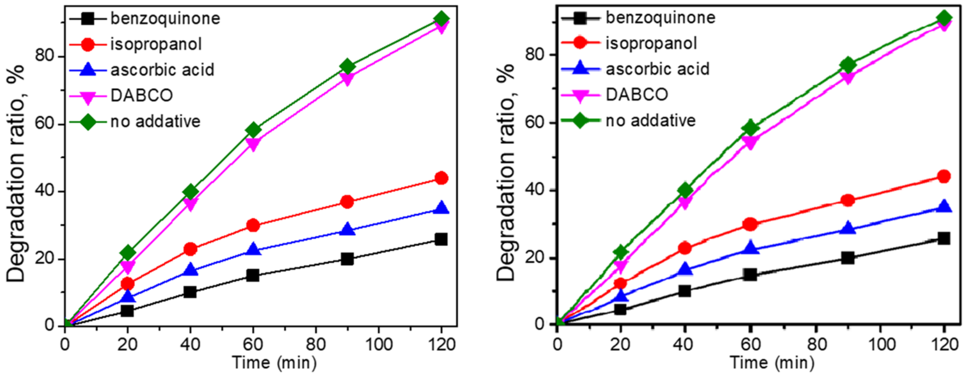

Fig. 11 The effects of the quenchers (0.5 mM) on the photo-degradation of BPB

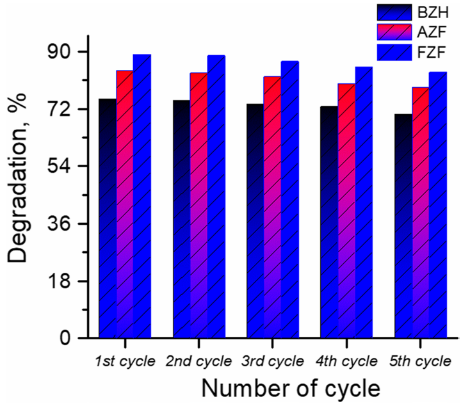

Fig. 12 The recycling experiment of $ZnFe_2O_4$ NPs in the degradation of BPB dye

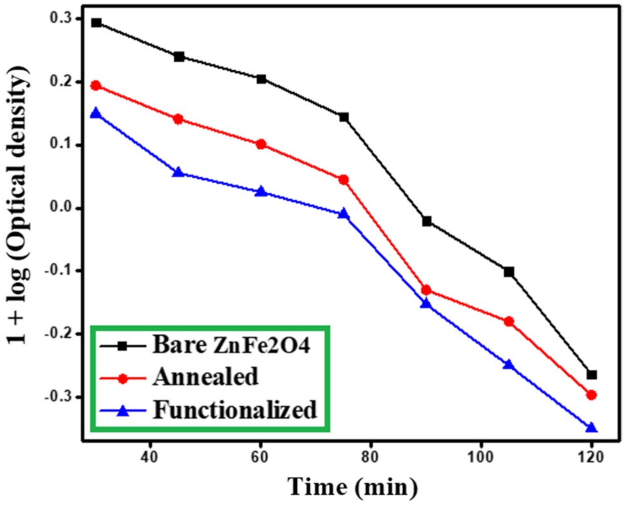

Fig. 13 Reaction kinetics of the degradation of BPB

The photocatalytic activity of all three types of photocatalysts can also be calculated using relationship (Ali et al. 2020c).

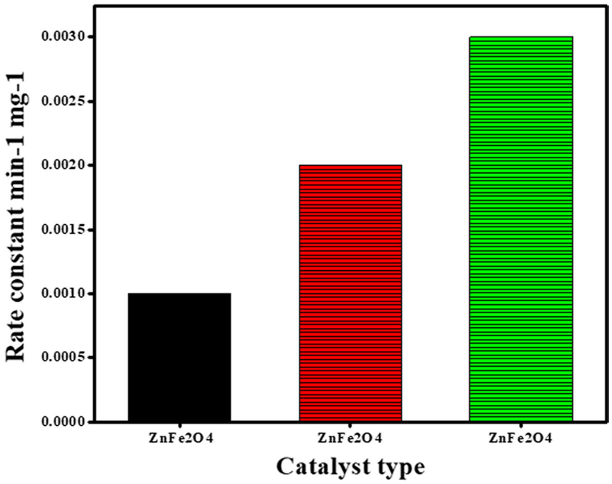

Fig. 14 Decolorization rate of $ZnFe_2O_4$ photocatalyst

$$\text{Catalytic efficiency} = k/C_{\text{cat}} \tag{2}$$

where k is rate constant, and C_{cat} is the amount of catalyst. The modified $ZnFe_2O_4$ NPs have a smaller grain size and higher catalytic activity due to many active sites. The degradation rates of $ZnFe_2O_4$ NPs (bare, calcined, and modified) were determined by using rate constants that were achieved from the slope of kinetics plots. The degradation rate of all three types of $ZnFe_2O_4$ NPs is illustrated in Fig. 14. The photocatalytic degradation of BPB dye in the presence of modified $ZnFe_2O_4$ was higher than bare and calcined $ZnFe_2O_4$ NPs. The greater performance of modified $ZnFe_2O_4$ NPs is due to the existence of a greater number of active sites.

Conclusion

Zinc ferrite ($ZnFe_2O_4$) NPs were successfully prepared via the co-precipitation route, and their surface was successfully modified with 0.1 M of 3-(APTES) solution. FT-IR analysis confirmed that the 3-APTES is well grafted on the surface of $ZnFe_2O_4$ NPs. The XRD analysis shows the crystalline structure in calcined and modified $ZnFe_2O_4$ NPs, while the amorphous nature of bare $ZnFe_2O_4$ NPs was observed. The SEM micrographs displayed a flat surface morphology with almost monodispersed grain size and irregular shape structure for all $ZnFe_2O_4$ NPs. The grain size of the synthesized $ZnFe_2O_4$ NPs was found to be 106.5, 23.3, and 13.9 nm for bare, calcined, and modified $ZnFe_2O_4$ NPs, respectively. Optical band gap energy was calculated in both acidic (2.47 eV) and basic medium (2.7 eV) using a taulc plot. The photocatalytic performance of $ZnFe_2O_4$ NPs exhibits that the modified $ZnFe_2O_4$ degrade 95.4% of BPB dye at pH 12 in 120 min. The rate of BPB dye degradation on the surface of $ZnFe_2O_4$ NPs followed pseudo 1st order of kinetics model ($k = 6.7 \times 10^{-3}$/sec). The photocatalytic degradation efficiency were 0.0011 min^{-1} mg^{-1} (bare), 0.0012 min^{-1} mg^{-1} (calcined) and 0.0015 min^{-1} mg^{-1} (modified) $ZnFe_2O_4$ NPs, respectively. The degradation rate for the removal of BPB dye in the presence of modified $ZnFe_2O_4$ catalyst was found to be greater than bare and calcined $ZnFe_2O_4$ photocatalyst.

Acknowledgments The authors wish to thank all who assisted in conducting this work.

Authors contribution FA: Conceptualization, Data analysis and curation, Project administration, Supervision, Validation, Writing—original draft, review & editing. LF, AS, NT, FR: Investigation, Methodology, Data analysis and curation. UA, MSA: Validation, Writing—review & editing. AR: Data analysis, Writing—review & editing. NA: Formal analysis, Writing—review & editing. NA, MB: Data analysis, Formal analysis, Writing—review & editing.

Funding The financial supporters of this work are "National & Local Joint Engineering Research Center for Mineral Salt Deep Utilization (No. SF 202109)".

Declarations

Conflict of interest The authors declare that they have no conflict of interest.

References

Akpan UG, Hameed BH (2009) Parameters affecting the photocatalytic degradation of dyes using TiO2-based photocatalysts: a review. J Hazard Mater 170(2–3):520–529. https://doi.org/10.1016/j.jhazmat.2009.05.039

Ali N, Ali F, Said A et al (2020a) Characterization and deployment of surface: engineered cobalt ferrite nanospheres as photocatalyst for highly efficient remediation of alizarin red S dye from aqueous solution. J Inorg Organomet Polym Mater. https://doi.org/10.1007/s10904-020-01654-y

Ali F, Ali N, Altaf M, Said A, Shah SS, Bilal M (2020b) Epoxy polyamide composites reinforced with silica nanorods: fabrication, thermal and morphological investigations. J Inorg Organomet Polym Mater. https://doi.org/10.1007/s10904-020-01518-5

Ali N, Said A, Ali F et al (2020c) Photocatalytic degradation of congo red dye from aqueous environment using cobalt ferrite nanostructures: development, characterization, and photocatalytic performance. Water Air Soil Pollut. https://doi.org/10.1007/s11270-020-4410-8

Ali N, Said A, Ali F, Khan M, Sheikh ZA, Bilal M (2020d) Development and characterization of functionalized titanium dioxide-reinforced sulfonated copolyimide (SPI/TiO_2) nanocomposite membranes with improved mechanical, thermal, and electrochemical properties. J Inorg Organomet Polym Mater. https://doi.org/10.1007/s10904-020-01636-0

Ameen S, Akhtar MS, Seo HK, Shin HS (2014) Solution processed CeO_2/TiO_2 nanocomposite as potent visible light photocatalyst for the degradation of BPB dye. Chem Eng J 247:193–198

Anchieta C, Cancelier A, Mazutti M et al (2014) Effects of solvent diols on the synthesis of ZnFe2O4 particles and their use as heterogeneous Photo-Fenton catalysts. Materials (basel) 7(9):6281–6290. https://doi.org/10.3390/ma7096281

Bouanimba N, Zouaghi R, Laid N, Sehili T (2011) Factors influencing the photocatalytic decolorization of Bromophenol blue in aqueous solution with different types of TiO2 as photocatalysts. Desalination 275(1–3):224–230. https://doi.org/10.1016/j.desal.2011.03.005

Buthiyappan A, Abdul Raman AA, Daud WMAW (2016) Development of an advanced chemical oxidation wastewater treatment system for the batik industry in Malaysia. RSC Adv 6(30):25222–25241. https://doi.org/10.1039/c5ra26775g

Cao SW, Zhu YJ, Cheng GF, Huang YH (2009) $ZnFe_2O_4$ nanoparticles: microwave-hydrothermal ionic liquid synthesis and photocatalytic property over phenol. J Hazard Mater 171(1–3):431–435. https://doi.org/10.1016/j.jhazmat.2009.06.019

Dehghani MH, Dehghan A, Alidadi H, Dolatabadi M, Mehrabpour M, Converti A (2017) Removal of methylene blue dye from aqueous solutions by a new chitosan/zeolite composite from shrimp waste: kinetic and equilibrium study. Korean J Chem Eng 34(6):1699–1707. https://doi.org/10.1007/s11814-017-0077-2

Dhiman M, Sharma R, Kumar V, Singhal S (2016) Morphology controlled hydrothermal synthesis and photocatalytic properties of ZnFe2O4 nanostructures. Ceram Int 42(11):12594–12605. https://doi.org/10.1016/j.ceramint.2016.04.115

Dlamini LN, Krause RW, Kulkarni GU, Durbach SH (2011) Photodegradation of bromophenol blue with fluorinated TiO2 composite. Appl Water Sci 1(1–2):19–24. https://doi.org/10.1007/s13201-011-0004-3

Emmanuel KT, Sudesh R (2021) Adsorption and photocatalytic mineralization of bromophenolblue dye with TiO_2 modified with clinoptilolite/activated carbon. Catalysts MDPI 11:7. https://doi.org/10.3390/catal11010007

Fan GL, Gu ZJ, Yang L, Li F (2009) Nanocrystalline zinc ferrite photocatalyst formed using the colloid mill and hydrothermal technique. Chem Eng J 155:534–541

Fu YS, Wang X (2011) Magnetically separable $ZnFe_2O_4$ graphene catalyst and its high photocatalytic performance under visible light irradiation. Ind Eng Chem Res 50:7210–7218

Fuku X, Matinise N, Masikini M, Kasinathan K, Maaza M (2017) An electrochemically active green synthesized polycrystalline NiO/MgO catalyst: use in photocatalytic applications. Mater Res Bull 2018(97):457–465. https://doi.org/10.1016/j.materresbull.2017.09.022

Haider S, Bukhari N, Park SY, Iqbal Y, Al-Masry WA (2011) Adsorption of bromo-phenol blue from an aqueous solution onto thermally modified granular charcoal. Chem Eng Res Des 89(1):23–28. https://doi.org/10.1016/j.cherd.2010.04.022

Hankare PP, Patil RP, Jadhav AV, Garadkar KM, Sasikala R (2011) Enhanced photocatalytic degradation of methyl red and thymol blue using titania-alumina-zinc ferrite nanocomposite. Appl Catal

B Environ 107(3–4):333–339. https://doi.org/10.1016/j.apcatb.2011.07.033

He Y, Dai C, Zhou X (2017) Magnetic cobalt ferrite composite as an efficient catalyst for photocatalytic oxidation of carbamazepine. Environ Sci Pollut Res 24(2):2065–2074. https://doi.org/10.1007/s11356-016-7978-1

Jadhav SD, Hankare PP, Patil RP, Sasikala R (2011) Effect of sintering on photocatalytic degradation of methyl orange using zinc ferrite. Mater Lett 65(2):371–373. https://doi.org/10.1016/j.matlet.2010.10.004

Jayaraman A, Mas S, Tauler R, de Juan A (2012) Study of the photodegradation of 2-bromophenol under UV and sunlight by spectroscopic, chromatographic and chemometric techniques. J Chromatogr B Anal Technol Biomed Life Sci 910:138–148. https://doi.org/10.1016/j.jchromb.2012.03.038

Jia Z, Ren D, Liang Y, Zhu R (2011) A new strategy for the preparation of porous zinc ferrite nanorods with subsequently light-driven photocatalytic activity. Mater Lett 65(19–20):3116–3119. https://doi.org/10.1016/j.matlet.2011.06.101

Khan A, Wahid F, Ali N, Badshah S, Airoldi C (2015) Single-step modification of chitosan for toxic cations remediation from aqueous solution. Desalin Water Treat 56(4):1099–1109. https://doi.org/10.1080/19443994.2014.944575

Khan H, Khalil AK, Khan A, Saeed K, Ali N (2016) Photocatalytic degradation of bromophenol blue in aqueous medium using chitosan conjugated magnetic nanoparticles. Korean J Chem Eng 33(10):2802–2807. https://doi.org/10.1007/s11814-016-0238-8

Li X, Zhao Q, Quan X (2010) New photocatalyst electrodes and their photocatalytic degradation properties of organics. Curr Org Chem 14(7):709–727. https://doi.org/10.2174/138527210790963412

Li X, Hou Y, Zhao Q, Wang L (2011) A general, one-step and template-free synthesis of sphere-like zinc ferrite nanostructures with enhanced photocatalytic activity for dye degradation. J Colloid Interface Sci 358(1):102–108. https://doi.org/10.1016/j.jcis.2011.02.052

Magdalane CM, Kaviyarasu K, Vijaya JJ et al (2017) Evaluation on the heterostructure CeO2/Y2O3 binary metal oxide nanocomposites for UV/Vis light induced photocatalytic degradation of Rhodamine-B dye for textile engineering application. J Alloys Compd 727:1324–1337. https://doi.org/10.1016/j.jallcom.2017.08.209

Mohsen VN, Razieh SK, Davoud SK (2021) Enhanced photocatalyst activity of Ni-doped $BiFeO_3$ nanoparticles for degradation of bromophenol blue (BPB) in aqueous solutions. J React Kinet Mech Catal 134:951–970. https://doi.org/10.1007/s11144-021-02102-9

Nezamzadeh-Ejhieh A, Banan Z (2011) A comparison between the efficiency of CdS nanoparticles/zeolite A and CdO/zeolite A as catalysts in photodecolorization of crystal violet. Desalination 279(1–3):146–151. https://doi.org/10.1016/j.desal.2011.06.006

Nezamzadeh-Ejhieh A, Banan Z (2012) Sunlight assisted photodecolorization of crystal violet catalyzed by CdS nanoparticles embedded on zeolite A. Desalination 284:157–166. https://doi.org/10.1016/j.desal.2011.08.050

Nezamzadeh-Ejhieh A, Moazzeni N (2013) Sunlight photodecolorization of a mixture of Methyl Orange and Bromocresol green by CuS incorporated in a clinoptilolite zeolite as a heterogeneous catalyst. J Ind Eng Chem 19(5):1433–1442. https://doi.org/10.1016/j.jiec.2013.01.006

Posa VR, Annavaram V, Koduru JR, Ammireddy VR, Somala AR (2016) Graphene-ZnO nanocomposite for highly efficient photocatalytic degradation of methyl orange dye under solar light irradiation. Korean J Chem Eng 33(2):456–464. https://doi.org/10.1007/s11814-015-0145-4

Rauf MA, Ashraf SS (2009) Radiation induced degradation of dyes-an overview. J Hazard Mater 166(1):6–16. https://doi.org/10.1016/j.jhazmat.2008.11.043

Rishikeshi SN, Joshi SS, Temgire MK, Bellare JR (2013) Chain length dependence of polyol synthesis of zinc ferrite nanoparticles: why is diethylene glycol so different? Dalt Trans 42(15):5430–5438. https://doi.org/10.1039/c2dt32026f

Ruttink PJA, Dekker LJM, Luider TM, Burgers PC (2012) Complexation of divalent metal ions with diols in the presence of anion auxiliary ligands: zinc-induced oxidation of ethylene glycol to glycolaldehyde by consecutive hydride ion and proton shifts. J Mass Spectrom 47(7):869–874. https://doi.org/10.1002/jms.3039

Sakthivel S, Neppolian B, Shankar MV, Arabindoo B, Palanichamy M, Murugesan V (2003) Solar photocatalytic degradation of azo dye: comparison of photocatalytic efficiency of ZnO and TiO_2. Sol Energy Mater Sol Cells 77(1):65–82. https://doi.org/10.1016/S0927-0248(02)00255-6

Sehar S, Naz I, Perveen I, Ahmed S (2019) Superior dye degradation using SnO2-ZnO hybrid heterostructure catalysts. Korean J Chem Eng 36(1):56–62. https://doi.org/10.1007/s11814-018-0159-9

Shah T, Gul T, Saeed K (2019) Photodegradation of BPB in aqueous medium using graphene nanoplates-supported TiO_2. Appl Water Sci 9(4):1–7

Shams-Ghahfarokhi Z, Nezamzadeh-Ejhieh A (2015) As-synthesized ZSM-5 zeolite as a suitable support for increasing the photoactivity of semiconductors in a typical photo-degradation process. Mater Sci Semicond Process 39:265–275. https://doi.org/10.1016/j.mssp.2015.05.022

Skrabalak SE, Wiley BJ, Kim M, Formo EV, Xia Y (2008) On the polyol synthesis of silver nanostructures: glycolaldehyde as a reducing agent. Nano Lett 8(7):2077–2081. https://doi.org/10.1021/nl800910d

Srinivasan SS, Wade J, Stefanakos EK (2006) Synthesis and characterization of photocatalytic TiO_2 - $ZnFe_2O_4$ nanoparticles. J Nanomater. https://doi.org/10.1155/JNM/2006/45712

Tashtoush AM (2021) Non-invasive blood glucose measurement using laser technology (NIBGM). Int J Comput Digit Syst 10(1):297–307

Tourinho F, Franck R, Massart R, Perzynski R (2007) Synthesis and mangeitc properties of managanese and cobalt ferrite ferrite ferrofluids. Trends Colloid Interface Sci 134:128–134. https://doi.org/10.1007/bfb0116198

Ullah I, Ali F, Ali Z, Humayun M, Wahab ZU (2018) Glycol stabilized magnetic nanoparticles for photocatalytic degradation of xylenol orange. Mater Res Express. https://doi.org/10.1088/2053-1591/aac3b8

Valizadeh S, Rasoulifard MH, Dorraji MSS (2016) Adsorption and photocatalytic degradation of organic dyes onto crystalline and amorphous hydroxyapatite: optimization, kinetic and isotherm studies. Korean J Chem Eng 33(2):481–489. https://doi.org/10.1007/s11814-015-0172-1

Wu Q, Zhang H, Zhou L, Bao C, Zhu H, Zhang Y (2016) Synthesis and application of rGO/CoFe2O4 composite for catalytic degradation of methylene blue on heterogeneous Fenton-like oxidation. J Taiwan Inst Chem Eng 67:484–494. https://doi.org/10.1016/j.jtice.2016.08.004

Xie YB, Li XZ (2006) Interactive oxidation of photoelectrocatalysis and electro-Fenton for azo dye degradation using TiO_2-Ti mesh and reticulated vitreous carbon electrodes. Mater Chem Phys 95(1):39–50. https://doi.org/10.1016/j.matchemphys.2005.05.048

Xie T, Liu C, Xu L, Yang L, Zhou W (2013) Novel heterojunction $Bi_2O_3/SrFe_{12}O_{19}$ magneticphotocatalyst with highly enhanced photocatalytic activity. J Phys Chem C 117(46):24601–24610. https://doi.org/10.1021/jp408627e

Yang J, Cui S, Qiao JQ, Lian HZ (2014) The photocatalytic dehalogenation of chlorophenols and bromophenols by cobalt doped nano TiO_2. J Mol Catal A Chem 395:42–51. https://doi.org/10.1016/j.molcata.2014.08.001

Authors and Affiliations

L. Fei[1] · F. Ali[2] · A. Said[2] · N. Tariq[2] · F. Raziq[3] · N. Ali[1] · U. Arif[2] · M. S. Akhter[4] · A. Rahdar[5] · M. Bilal[6]

[1] National & Local Joint Engineering Research Center for Mineral Salt Deep Utilization, Huaiyin Institute of Technology, Huaian 223003, People's Republic of China

[2] Department of Chemistry, Hazara University, Mansehra 21300, KPK, Pakistan

[3] School of Physics, University of Electronic Science and Technology of China, Chengdu 610054, People's Republic of China

[4] Department of Chemistry, College of Science, University of Bahrain, Zallaq, Bahrain

[5] Department of Physics, University of Zabol, P. O. Box. 98613-35856, Zabol, Iran

[6] School of Life Science and Food Engineering, Huaiyin Institute of Technology, Huaian 223003, China